vegetation parameters cci

CCI Vegetation

D2.1 Algorithm Theoretical Basis Document Retrieval Algorithm Cycle 2

Simon Blessing

November 2025

Distribution list

Author(s)	:	Simon Blessing
Reviewer(s)	:	Else Swinnen, Christiaan Van der Tol
Approver(s)	:	Marin Tudoroiu
Issuing authority	:	VITO

Change record

Release	Date	Pages	Description of change	Editor(s)/Reviewer(s)
V1	03/09/2022	all	First version	Simon Blessing / Else Swinnen
V2	13/11/2024	multiple	Cycle 2/CRDP-2; added mixed prior approach	Simon Blessing / Else Swinnen
V2.1	30/09/2025	p. 2 p. 8 Table 1 p. 17 p. 21 p. 21 p. 23-31 Multiple pages	Update Executive summary Update version number OptiSAIL Correction for Metop-B and C Update on Mixed prior extension Update on RETR_UNTRUSTED Treatment of RETR_GAP_FILLED Results of the scenario evaluation was added Edits	Simon Blessing / Fernando Camacho / Else Swinnen
V2.2	19/11/2025	p. 17, 20 p. 27 p. 30	Equation numbering adapted. Edits Explanation on 15 tiles processing added	Simon Blessing, Else Swinnen

Executive summary

CCI+ Vegetation Parameters is part of the ESA Climate Change Initiative. It aims at the identification, development and improvement of algorithms for the consistent retrieval of vegetation ECVs LAI and fAPAR from multi-platform and multi-mission satellite data, the generation of long-term climate data records, and the interaction with the user community to match their requirements. The work plan includes three cycles, in which different data sources are combined, the algorithms' scientific and operational maturity is increased, and user feedback is incorporated.

This document is an updated version of the D2.1 ATBD V1.2. It describes the OptiSAIL algorithm used in cycle 2 and its application to TOC reflectances from multiple sensors. During cycle-1, the OptiSAIL cloud contamination simulation was activated, and a pre-filtering algorithm was implemented. As a reaction to user preferences, the fAPAR absorbed by Chlorophyll A+B (fAPAR_Cab) is computed as additional output of OptiSAIL. The version for cycle-2 uses the posterior covariance matrix of the previous retrieval at the same location to modify the prior assumption, thus introducing a temporal correlation in the data, based on the assumption that the model variables have individual timescales on which they change. Also, with the simultaneous use of additional sensors, it became necessary to add a concept to balance prior and data term in the minimisation.

Table of Contents

LIST OF ACRONYMS

BHR	Bi-hemispherical Reflectance
BRDF	Bi-directional Reflectance Distribution Function
BRF	Bi-directional reflectance factor
CCI+	Climate Change Initiative Plus
DHR	Directional-Hemispherical reflectance
ECV	Essential Climate Variable
ED	External Document (as listed in section 1.2)
EOF	Empirical Orthogonal Function
fAPAR	***f***raction of Absorbed Photosynthetically Active Radiation
HDR	Hemispherical-Directional reflectance
ID	Internal Document (as listed in section 1.2)
LAI	Leaf Area Index
NIR	Near Infra-Red range of the electromagnetic spectrum, here 700--2500 nm
PCA	Principal Components Analysis
PROSPECT	PROperties of leaf SPECTtra
RT	Radiative Transfer
SAIL	Scattering of Arbitrarily Inclined Leaves
TAF	Transformation of Algorithms in Fortran
TARTES	Two-streAm Radiative TransfEr in Snow
TOA	Top-Of-Atmosphere
TOC	Top-Of-Canopy
VIS	VISible range of the electromagnetic spectrum, here 400–700 nm
VP	Vegetation Parameters

LIST OF FIGURES

LIST OF TABLES

1 Introduction

1.1 Scope of this document

This document updates the theoretical basis of the algorithms (ATBD-V1.1) used in cycle 1 of the CCI+ Vegetation Parameters project (ID1) for the production of the CRDP-2 with processor version OptiSAIL-r39528M. The OptiSAIL algorithm retrieves LAI and fAPAR together with other parameters directly from TOC reflectances. Because OptiSAIL includes turbid-medium radiative transfer model and does not account for horizontal sub-pixel heterogeneity, the LAI is an effective LAI that disregards possible effects of vegetation clumping (partial vegetation coverage and shoot, branch and crown clumping).

1.2 Related documents

Internal documents

Reference ID	Document
ID1	Climate Change Initiative Extension (CCI+) Phase 2 New ECVs: Vegetation Parameters – EXPRO+ (ITT) + - Statement of Work, prepared by ESA Climate Office, Reference ESA-EOP-SC-CA-2021-7, Issue 1.2, date of issue 26/05/2021
VP-CCI_D1.1_URD_V2.0	User Requirement Document: fAPAR and LAI, ESA CCI+ Vegetation Parameters https://climate.esa.int/media/documents/VP-CCI_D1.1_URD_V2.0.pdf
VP-CCI_D4.2_PUG_V2.2	Product User Guide: LAI and fAPAR, ESA CCI+ Vegetation Parameters http://climate.esa.int/media/documents/VP-CCI_D4.2_PUG_V2.2.pdf
VP-CCI_D2.4_PVASR_V1.0	Product Validation and Algorithm Selection Report: fAPAR and LAI, ESA CCI+ Vegetation Parameters http://climate.esa.int/media/documents/VP-CCI_D2.4_PVASR_V1.1.pdf
VP-CCI_D4.1_PVIR_V2.1	Product Validation and Intercomparison Report: fAPAR and LAI, ESA CCI+ Vegetation Parameters http://climate.esa.int/media/documents/VP-CCI_D4.1_PVIR_V2.1.pdf
VP-CCI_D2.1_ATBD-pre-processing_V1	Algorithm Theoretical Basis Document – Cycle-2 pre-processing https://climate.esa.int/media/documents/VP-CCI_D2.1_ATBD_pre-processing_v1.0.pdf

External documents

Reference ID	Document
ED1	C3S ATBD of Surface Albedo, multi-sensor, D1.3.4-v2.0_ATBD_CDR_SA_MULTI_SENSOR_v2.0_PRODUCTS_v1.1
ED2	CGLS ATBD Sentinel-3 OLCI and SLSTR atmospheric correction , CGLOPS1_ATBD_S3-AC-V1_I1.30

1.3 General definitions

Leaf Area Index (LAI) is defined as the total one-sided area of all leaves in the canopy within a defined region, and is a non-dimensional quantity, although units of [m2/m2] are often quoted, as a reminder of its meaning (Zemp et al., 2022). The selected algorithm in the CCI-Vegetation Parameters project uses a 1-D radiative transfer model, and LAI is uncorrected for potential effects of crown clumping. Its value can be considered as an effective LAI, notably the LAI-parameter of a turbid-medium model of the canopy that would let the model have similar optical properties as the true 3-D structured canopy with true LAI (Pinty et al., 2006). Additional information about the geometrical structure may be required for this correction to obtain true LAI (Nilson, 1971), which involves the estimation of the clumping index, CI, defined as the ratio between the true and effective LAI [see Fang (2021) for a review of methods to estimate CI].

Fraction of Absorbed Photosynthetically Active Radiation (fAPAR) is defined as the fraction of Photosynthetically Active Radiation (PAR; solar radiation reaching the surface in the 400-700 nm spectral region) that is absorbed by a vegetation canopy (Zemp et al., 2022).

2 CRDP-2

For the production of the CRDP-2, the OptiSAIL algorithm was used, with some changes from the version used for CRDP-1. These are mainly the mixed prior approach described in section 4.2 and the use of data from more instruments. See Table 1 for the differences between the CRDP-1 inputs and the CRDP-2 input candidates. Section 5 presents the selected input data for CRDP-2. CRDP-2 contains a selection of data layers from OptiSAIL, applied to TOC reflectances retrieved with multiple combinations of sensors. This data is described in the PUG (VP-CCI_D4.2_PUG).

The input data availability per sensor is shown in Figure 1.

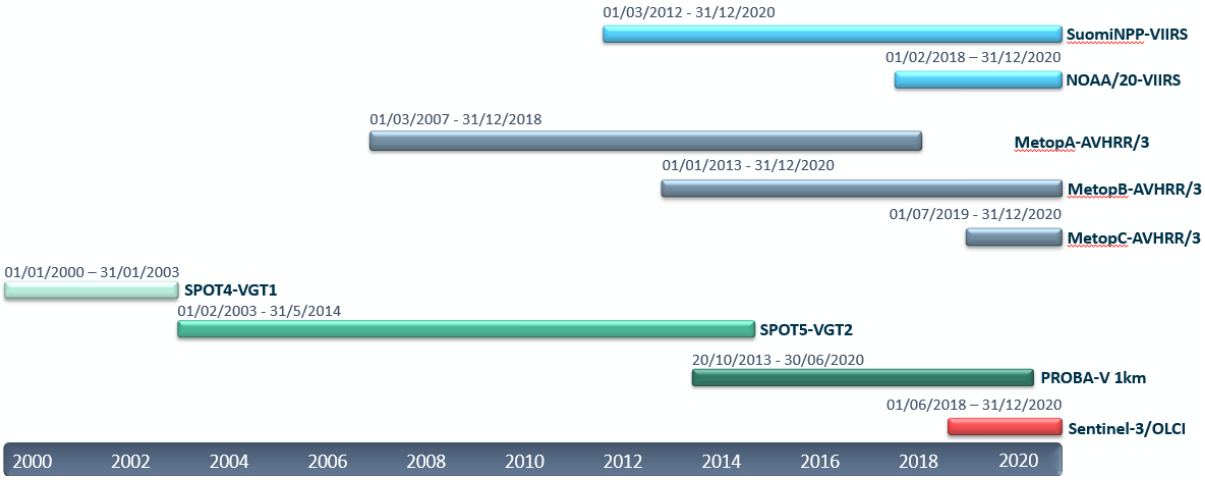

Figure 1: Input data availability per sensor.

Table 1: Differences of Inputs datasets prepared for use in CRDP-1 and CRDP-2.

Platform	Sensor	Band name In data	Central Wavelength of SRF (nm)	CRDP-1	CRDP-2 Candidate	band flags	Snow Identification	Cloud Identification	ac_flag (CRDP-2)	SZA/VZA filter (deg; CRDP-2)	remarks
METOP-A	AVHRR/3	TOC_1	633		x	NA	status_map is „ice_snow“	status_map is „cloudy“	Drop „Climato“	65/65	
		TOC_2	864		x	NA					
		TOC_3a	1606.5		x	NA					
METOP-B	AVHRR/3	TOC_1	633		(x)	NA	status_map is „ice_snow“	status_map is „cloudy“	Drop „Climato“	65/65	Unreliable geolocation
		TOC_2	862		(x)	NA					Unreliable geolocation
		TOC_3a	1607.5		(x)	NA					Unreliable geolocation
METOP-C	AVHRR/3	TOC_1	628.96		x	NA	status_map is „ice_snow“	status_map is „cloudy“	Drop „Climato“	65/65	
		TOC_2	837.81		x	NA					
		TOC_3a	1607.22		x	NA					
S-NPP	VIIRS	TOC_M01	410.57		x	TOC_Mnn_quality_flags is not any of „Substitute_Cal“ or „Out_of_Range“ or „Saturation“ or „Temp_not_Nominal“ or „DG_Anomaly“ or „Some_Saturation“ or „Missing_EV“ or „Cal_Fail“ or „Dead_Detector“ or „Noisy_Detector“	NA	Integer_Cloud_Mask is not any of „probably clear“ or „confident clear“	Drop „Climato“	65/65	
		TOC_M02	443.47		x						
		TOC_M03	486.19		x						
		TOC_M04	550.47		x						
		TOC_M05	671.25		x						
		TOC_M06	745.27		x						high uncertainty
		TOC_M07	861.61		x						
		TOC_M08	1238.26		x						
		TOC_M10	1601.16		x						
		TOC_M11	2256.99		x						
NOAA-20	VIIRS	TOC_M01	410.76		x	TOC_Mnn_quality_flags is not any of	NA	Integer_Cloud_Mask		65/65	

		TOC_M02	444.56		x	„Substitute_Cal“ or „Out_of_Range“ or „Saturation“ or „Temp_not_Nominal“ or „DG_Anomaly“ or „Some_Saturation“ or „Missing_EV“ or „Cal_Fail“ or „Dead_Detector“ or „Noisy_Detector“		is not any of „probably clear“ or „confident clear“	Drop „Climato“		
		TOC_M03	488.23		x						
		TOC_M04	558.48		x						
		TOC_M05	668.14		x						
		TOC_M06	745.88		x						high uncertainty
		TOC_M07	867.56		x						
		TOC_M08	1238.51		x						
		TOC_M10	1604.38		x						
		TOC_M11	2258.8		x						
PROBA-V	VNIR	LEVEL2B/band1/TOC	463.5	x	x	Good_Blue	SM_probav_v2 is „IceSnow“	SM_probav_v2 is „Shadow“ or „Undefined“ or „Cloud“	NA	65/65	
		LEVEL2B/band2/TOC	655	x	x	Good_Red					
		LEVEL2B/band3/TOC	839	x	x	Good_Nir					
	SWIR	LEVEL2B/band4/TOC	1602.5	x	x	none					Also use interpolated pixels
SPOT 4/VGT1	VEGETATION 1	LEVEL2B/band1/TOC	457.5	x	x	Good_Blue	SM is „IceSnow“	SM is „Shadow“ or „Undefined“ or „Cloud“	NA	65/65	
		LEVEL2B/band2/TOC	658.75	x	x	Good_Red					
		LEVEL2B/band3/TOC	833.75	x	x	Good_Nir					
		LEVEL2B/band4/TOC	1648.75	x	x	none					Also use interpolated pixels
SPOT 5/VGT2	VEGETATION 2	LEVEL2B/band1/TOC	457.5	x	x	Good_Blue	SM is „IceSnow“	SM is „Shadow“ or „Undefined“ or „Cloud“	NA	65/65	
		LEVEL2B/band2/TOC	653.75	x	x	Good_Red					
		LEVEL2B/band3/TOC	837.5	x	x	Good_Nir					
		LEVEL2B/band4/TOC	1635	x	x	none					Also use interpolated pixels

Sentinel -3A	OLCI	Oa02_toc	411.82		x	*Already Quality Screened*	Quality_flag is not any of „SNOW_ICE“ or „MIXED_CLEAR_SNOW_ICE“	*already Cloud Screened*	Drop „Climato“	65/65	
		Oa02_toc	442.95		x						
		Oa04_toc	490.45		x						
		Oa05_toc	510.42		x						
		Oa06_toc	560.43		x						
		Oa07_toc	620.38		x						
		Oa08_toc	665.24		x						
		Oa09_toc	674.01		x						
		Oa10_toc	681.56		x						
		Oa11_toc	709.12		x						
		Oa12_toc	754.18		x						
		Oa16_toc	779.22		x						
		Oa17_toc	865.59		x						
		Oa18_toc	884.36		x						
		Oa21_toc	1012.93		x						
Sentinel -3B	OLCI	Oa02_toc	411.94		x	Already Quality Screened	Quality_flag is not any of „SNOW_ICE“ or „MIXED_CLEAR_SNOW_ICE“	*already Cloud Screened*	Drop „Climato“	65/65	
		Oa02_toc	443.02		x						
		Oa04_toc	490.37		x						
		Oa05_toc	510.36		x						
		Oa06_toc	560.35		x						
		Oa07_toc	620.25		x						
		Oa08_toc	665.1		x						
		Oa09_toc	673.86		x						
		Oa10_toc	681.38		x						
		Oa11_toc	708.97		x						
		Oa12_toc	754.03		x						
		Oa16_toc	779.09		x						
		Oa17_toc	865.43		x						
		Oa18_toc	884.19		x						
		Oa21_toc	1012.76		x						

3 Processing and input data

Figure 2 sketches the structure for algorithm development and successively increasing data complexity in the three development cycles of this project. Atmospherically corrected, gridded TOC reflectance data have been used as input. The processing chain resulting in these input data is described in the atmospheric correction and pre-processing ATBD [VP-CCI_D2.1_ATBD-pre-processing_V1.0]. In each cycle of the project, different satellite products have been used. Figure 2 gives an overview of the data use per period and per cycle. The TOC reflectance datasets which will be produced for this project in cycles 2 and 3 will use the same approach for atmospheric correction as the products used in cycle 1.

Figure 3 gives an overview of the processing structure. OptiSAIL uses a mechanism to select reflectance data from multiple sources for a given temporal aggregation window. To improve the temporal resolution for situations with many usable observations, the TOC reflectance uncertainties are inflated with a time-dependent factor ($f(\Delta t)$). It is exponential in time difference Δt between the window centre and the observation time, and 1 for Δt=0 and 2 for Δt =120h (5d), computed as $f(\Delta t) = 2^{\left(\frac{\Delta t}{120\,h}\right)}$, thus a doubling of the uncertainty per 5 days.

Cloud and quality flags of the data are used to exclude pixels from processing whenever they are raised. Snow flags are used to select a higher value of the snow prior in the inversion.

To avoid outliers in the observations, a pre-filtering criterion based on a maximum anisotropy threshold was implemented. Bright outliers are filtered out as follows: for all sensors with bands at wavelengths shorter than 650 nm (CRDP-1: 500 nm) the band with the shortest wavelength is selected for comparison. All reflectances at this band higher than two times the lowest reflectance at this band are excluded from the retrieval. For this comparison no angular effects are considered, that is, the reflectances are treated as if they were Lambertian. This is expected to avoid the use of observations that suffer from undetected cloud, high aerosol, or similar effects in the retrieval.

A second filtering step selects out of the remaining observations per band only those three closest in time to the centre date of the observation window. This helps to increase temporal resolution and processing speed, and somewhat limits the effect of unknown reflectance error correlations, which are currently not considered. In order to have a better constraint of the cloud thickness parameter, observations are grouped together when they have an observation time that lies within the same period of 5 minutes. This can have the effect that more than three observations on the same band of one sensor can be used for the retrieval.

A common land sea mask is used for all TOC input datasets to define if a pixel is processed or not. The land-sea mask is derived from the ESA Sentinel-3 OLCI surface classification but resampled to 1 km resolution. All pixels with a fraction of 0.3 land cover are classified as land.

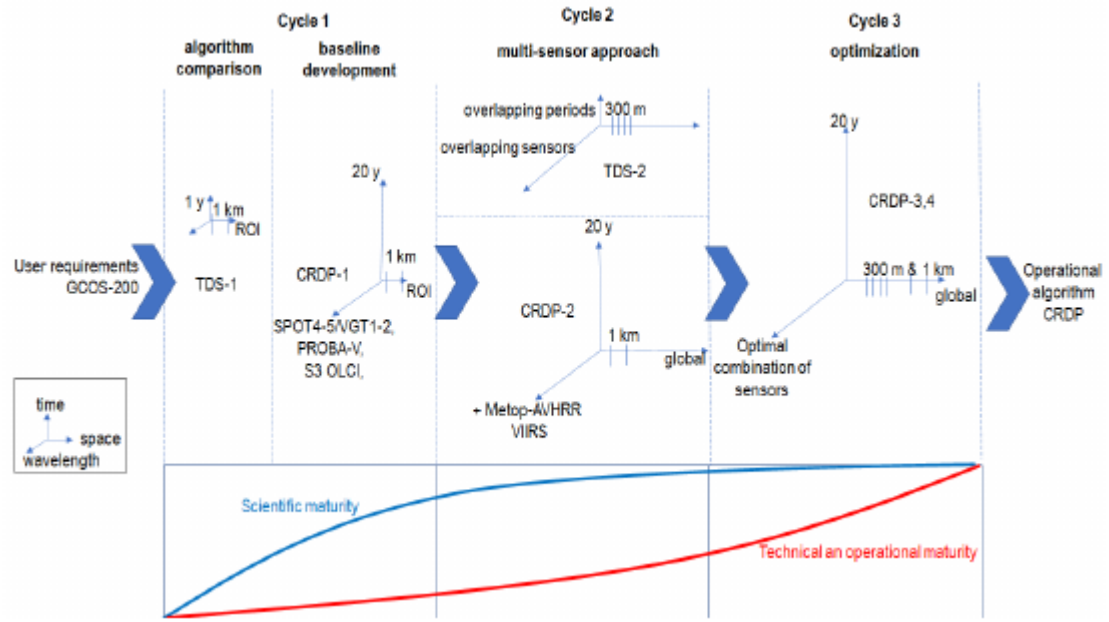

Figure 2: General concept of the three cycles, with progressive inclusion of sensors, spatial and temporal coverage and resolution, with the dimensions of the test datasets (TDS) and climate research data packages (CRDP) illustrated. The initially emphasis is on the implementation of an innovative approach, gradually shifting towards selection and optimization for an operational context.

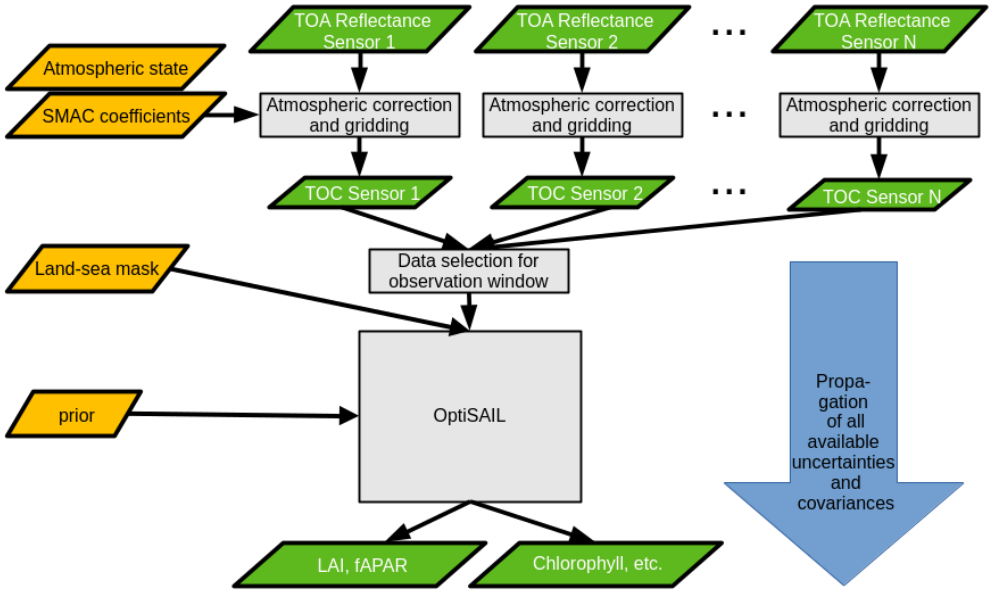

Figure 3: Processing diagram for CCI+ VP CRDP-2.

4 OptiSAIL

4.1 Algorithm Summary

OptiSAIL is a retrieval and error propagation framework. It uses automatic differentiation for gradient, Jacobian and Hessian computations. It is built around the established components 4SAILH (Scattering of Arbitrarily Inclined Leaves, with 4-stream extension and hot-spot), PROSPECT-D (simulation of leaf spectra, version D including senescence, (Féret et al., 2017), TARTES (Two-streAm Radiative Transfer in Snow (Libois et al., 2013), with the addition of an empirical soil reflectance model, a semi-empirical soil moisture model (Philpot, 2010), the Ross-Thick-Li-Sparse BRDF model, and a cloud contamination simulation. Table 2 shows the parameters of all sub-models that are retrieved simultaneously, and Figure 4 their prior distribution. In addition to the data pre-filtering for bright outliers in the band with the shortest wavelength less than 500 nm mentioned in section 2, the cloud contamination detection built into OptiSAIL (Blessing et al., 2024) was extended for the multi-sensor approach. It identifies and to some degree corrects for observations with residual cloud contamination. Test runs during cycle-1 showed quality issues when this option was not used.
Figure 5 gives an overview of the reflectance simulation and Figure 6 of the retrieval framework. The model is described with further references and demonstrated in (Blessing et al., (2024).

Table 2: OptiSAIL retrieved parameters by sub-model.

Parameter	Description	unit
	Cloud contamination sub-model	
L	Cloud thickness parameter vector (one entry per retrieval time)	m
	SAIL sub-model	
LAI	Leaf Area Index	m^2/m^2
ALIA	Average Leaf Inclination Angle (normal against zenith)	°
hspot	canopy hot-spot parameter	1
	PROSPECT-D sub-model	
N	leaf structure parameter	1
C_{ab}	chlorophyll a+b content	$\mu g/cm^2$
C_{Car}	carotenoids content	$\mu g/cm^2$
C_{Anth}	Anthocyanin content	$\mu g/cm^2$
C_{brown}	brown pigments content	1
C_w	equivalent water thickness	cm
C_m	dry matter content	g/cm^2
	Soil BRDF sub-model (Ross-Li-R)	
f_{vol}	volumetric scattering kernel factor	1
f_{geo}	geometric scattering kernel factor	1
	Snow sub-model (TARTES)	
h_{snow}	height of a single snow layer with fixed properties	1
	Soil albedo model (empirical+Philpot)	
EOF1	factor for empirical soil spectrum variation 1	1
EOF2	factor for empirical soil spectrum variation 2	1
moist	relative moisture saturation of soil (to field capacity)	1

4.2 Mixed prior extension

In the algorithm for CRDP-1, the retrieval was carried out for all pixels independently of each other, allowing for high flexibility in the parallelisation. It can, however, be assumed that the retrieved parameters follow temporal dynamics which has typical time scales for changes, with dry soil spectra changing slowest, and cloud cover fastest. In the algorithm for CRDP-2, we use this information by

taking the previous retrieval as prior information. Based on the difference in retrieval time, each parameter is relaxed towards the standard prior with an individual time scale (Table 3) with the following formula:

$$x(\Delta t) = exp\left(-\frac{\Delta t}{\tau}\right) x_{previous} + \left(1 - exp\left(-\frac{\Delta t}{\tau}\right) x_{default\ prior}\right) \qquad \textit{Eq. 1}$$

For the elements of the prior covariance matrix, we then have:

$$K_{ij}^{x}(\Delta t) = exp\left(-\frac{\Delta t}{\tau_j}\right) K_{ij}^{x_{previous}}\ exp\left(-\frac{\Delta t}{\tau_i}\right) + \left(1 - exp\left(-\frac{\Delta t}{\tau_j}\right)\right) K_{ij}^{x_{default\ prior}} \left(1 - exp\left(-\frac{\Delta t}{\tau_i}\right)\right) \qquad \textit{Eq. 2}$$

The mixed-prior approach can be configured to be used with (used in CRDP-2) or without the covariance matrix of the previous retrieval. For the relaxation times τ we have used literature values of (Yang et al., 2021), which are based on expert knowledge, with few modifications. For the leaf chlorophyll content a lower τ was used, considering that rapid changes may occur at senescence. For the thickness of residual clouds a τ of zero was used and for snow a low τ of 1 day.
In some cases, this could trap the algorithm in extreme and unlikely parts of the parameter space. Therefore, some filtering is applied to the previous retrieval before it is used for the computation of the new prior. First, it is checked whether any flags are raised which indicate sub-optimal quality. In an optional second step, the relaxation time scales are relaxed for all leaf parameters if either the previous Cab retrieval is below -1.5 standard deviations or the leaf mass (Cm) parameter is below –1 standard deviation. In that case, the time scale is halved for –1 standard deviation of either Cab, Cm, or Cw, using the expression 2^(min(x_Cab,x_Cm,x_Cw), thus shifting the prior to the default prior in order to avoid trapping solutions
With the additional sensors used simultaneously in CRDP-2, it became necessary to introduce a concept for the balance between prior and data term. In theory, the data term would be scaled according to its information content by the observational covariance. However, this information is currently unavailable and would also have to contain the cross-sensor covariance. Therefore, an ad-hoc scaling is used, derived from the behaviour of a hypothetical *nxn* co-variance matrix with equal entries in the off diagonal, based on a correlation *r.* Compared to a purely diagonal covariance matrix, this would scale a cost function with factor 1/(r*(n-1)+1). In CRDP-2, this factor is applied to the data term of the cost function, with *n* being the number of observations. This factor is also used to reduce the assumed degrees of freedom for the Chi-square-statistics. Empirical tests have shown a good system behaviour for r=0.75.

*Table 3: Time scales in **days** used for τ in the equations for the mixed prior*

Cloud contamination sub-model	
L	0
SAIL sub-model	
LAI	30
ALIA	30
Hspot	30
PROSPECT-D sub-model	
N	60
C_{ab}	7.5
C_{Car}	30
C_{Anth}	30
C_{brown}	30

C_w	30
C_m	30
Soil BRDF sub-model (Ross-Li-R)	
f_{vol}	60
f_{geo}	60
Snow sub-model (TARTES)	
h_{snow}	1
Soil albedo model (empirical+Philpot)	
EOF1	60
EOF2	60
Moist	2

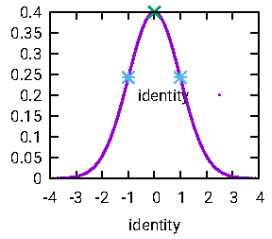

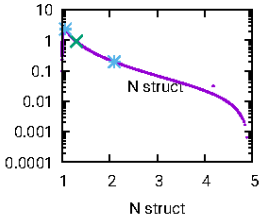

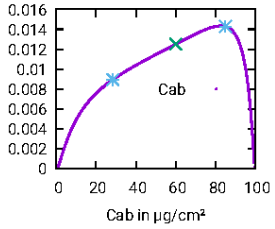

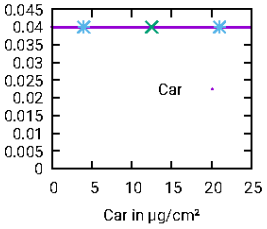

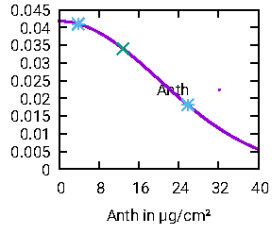

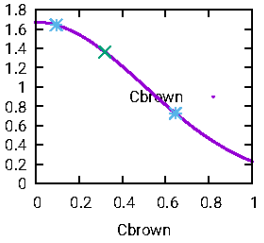

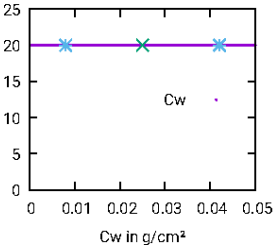

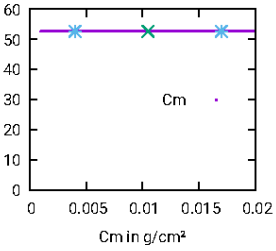

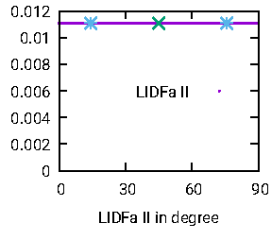

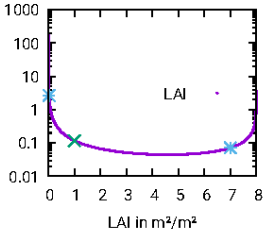

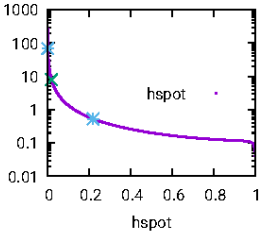

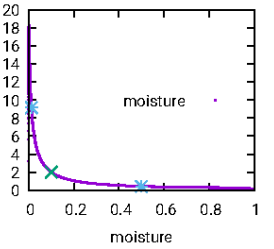

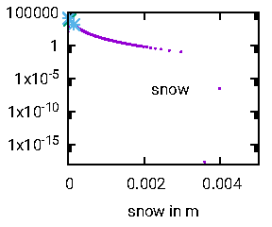

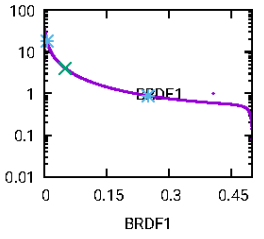

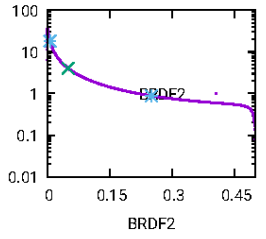

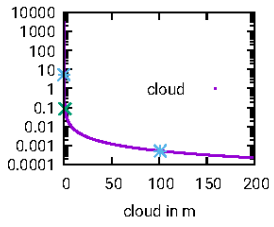

Figure 4: Prior distributions used in OptiSAIL. All model parameters are mapped to Gaussian control parameters for the minimisation, using these distributions.

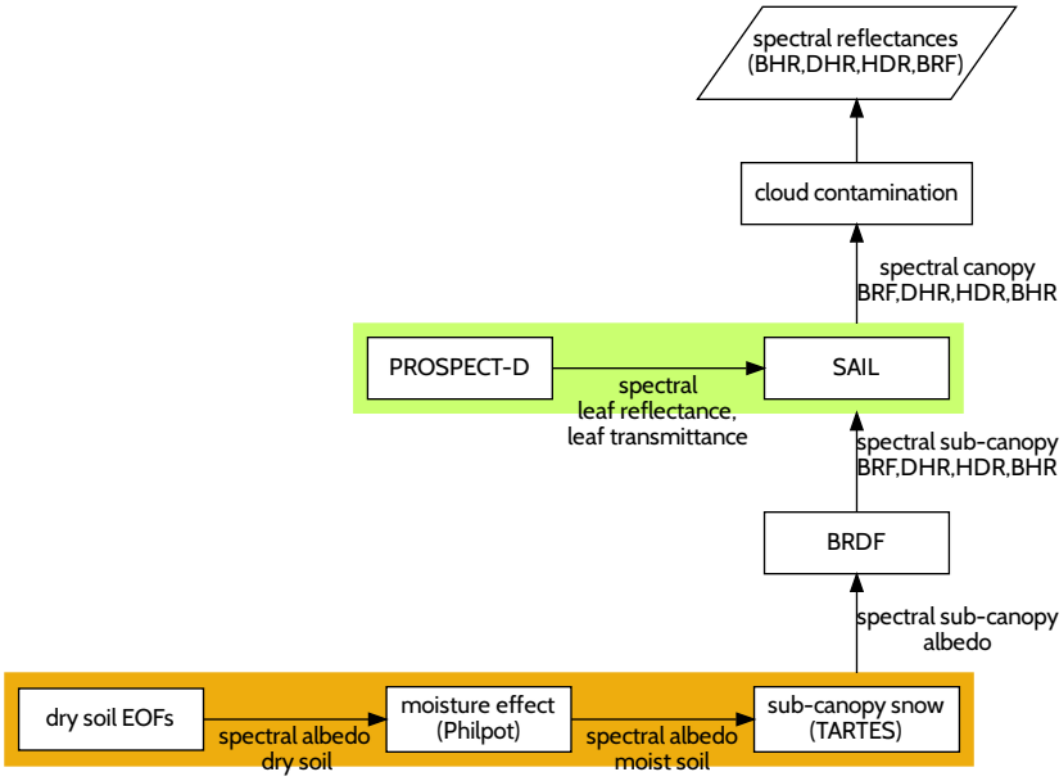

Figure 5: OptiSAIL reflectance simulation

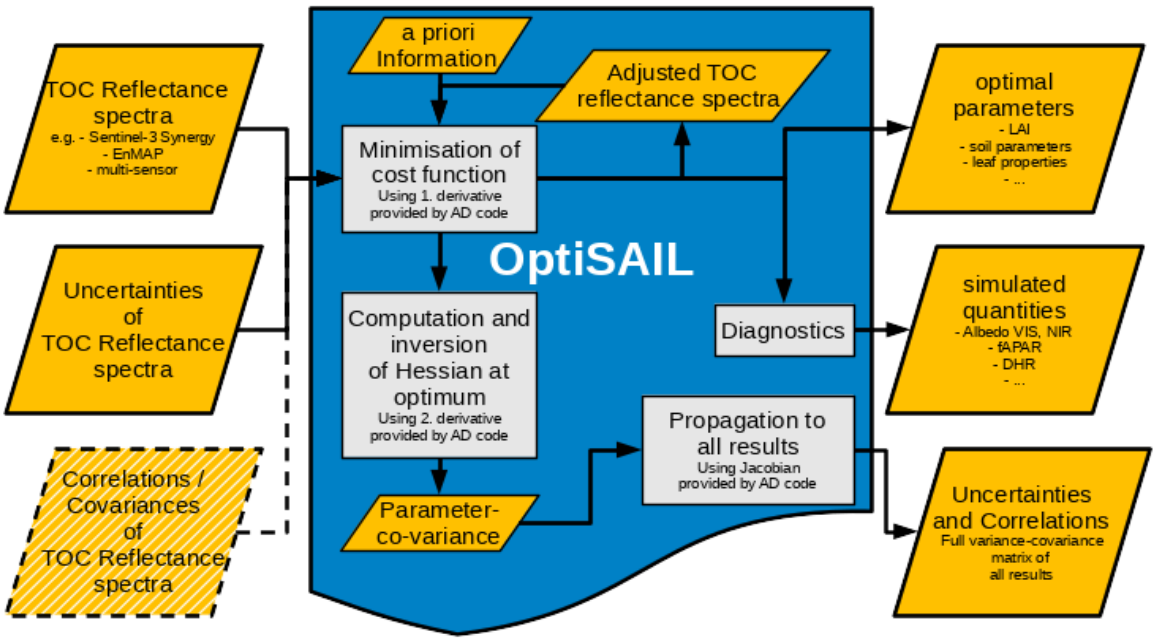

Figure 6: OptiSAIL retrieval framework with covariance propagation.

4.3 OptiSAIL output

All outputs for the CRDP-2 are on the same 1 km regular lat-lon grid as the TOC reflectance data used for input (ED1–3). The format is netCDF. For all retrieved and diagnosed quantities, the uncertainty corresponding to one standard deviation of a Gaussian distribution and the correlation of the uncertainty with all other retrieved and diagnosed quantities is given. In production, the correlation information can optionally be directed to a second output file. Table 4 gives an overview of the potential data layers. See the PUG (VP-CCI_D4.2_PUG) for the layers available to the user.

During cycle-1, the capability to compute fAPAR specifically absorbed by the leaf pigments Chlorophyll-A+B (*f*APAR_Cab) and Carotenoids (*f*APAR_Car) was added to OptiSAIL, by adopting the approach from SCOPE. In order to obtain the absorption by the pigment, the full leaf absorption spectrum (a_λ) is multiplied with the relative contribution to the total absorption of the respective pigment (Cab, Car):

$$a_{\lambda,pigment} = a_\lambda \frac{C_{pigment} \cdot k_{\lambda,pigment}}{\Sigma_{i=1}^{n} C_i k_{\lambda,i}} \qquad \text{Eq. 3}$$

The coefficient k_λ is the specific absorption coefficient as defined in PROSPECT-D, and *C* the pigment content. The summation in the denominator is over all pigments (van der Tol et al., 2019). Although the total absorption a_λ depends on many factors including multiple scattering between the soil and the vegetation, Eq. 3remains valid because the relative contribution to the absorption is conservative. Using ASTMG173 solar spectrum for the irradiance $E_{e,\lambda}$, *f*APAR_pigment is then computed as

$$fAPAR_{pigment} = \frac{\sum_{\lambda=400\,nm}^{700\,nm} a_\lambda E_{e,\lambda}}{\sum_{\lambda=400\,nm}^{700\,nm} E_{e,\lambda}} \qquad \text{Eq. 4}$$

In cycle-1 and 2, this sum is computed with 10 nm steps and an irradiance spectrum averaged over 10 nm-intervals, for computational speed.

Some additional layers exist, containing further information about the retrieval.

- "**n_bands_used**" gives the number of observations on individual bands, which were used in the inversion. Currently a cut-off of three observations per band and sensor is used to limit the influence of potential error correlations of data retrieved with the same sensor and platform or using the same ancillary data in the atmospheric correction, and to improve computational speed. For a sensor with four bands, for example, "n_bands_used" has a maximum value of 12 (=3*4).
- "**p_chisquare**" gives the probability of a χ^2-distribution with the same number of degrees of freedom as the retrieval, to have a cost function value greater or equal than the one reached in the inversion of the pixel ($p_{\chi^2}(J_{min,n}) = p(x \geq J_{min,n} | X \sim \chi^2_n)$). Low values of "p_chisquare" are an indicator that model and data are inconsistent, and hence the retrieval quality is low. In CRDP-1 and 2, retrievals with p_chisquare < 0.001 are discarded (invcode is set to "RETR_UNTRUSTED" and data to the missing value). Retrievals with 0.001<p_chisquare<0.01 are marked as "RETR_UNTRUSTED" in "invcode".

Quality flags are collected in "invcode" (Table 5). Those beginning with "OPTIERR" and "XHESSERR" are mainly of technical interest and are kept to identify eventual numerical issues. "RETR_UNTRUSTED" and "RETR_LOW_QUALITY" are intended as guidance for the user. "RETR_UNTRUSTED" can be raised with or without missing data values. If there is data, it should only be used with great caution (if at all).
"RETR_LOW_QUALITY" combines a number of criteria to identify unreliable or bad data. These criteria are:

- "RETR_UNTRUSTED" is raised
- cloud_thk > 2 m (median of cloud contamination over all observations is above 2 m of effective thickness; this was 1 m for the lowest contamination in CRDP-1)
- LAI > 3 and Chloropyll-A+B < 5 µg.cm-2 (dense canopy with extremely low Chlorophyll content, typically a bad solution triggered by complicated conditions, as varying snow cover during time window)
- LAI > 5 and Chloropyll-A+B < 15 µg.cm-2 (as above, but for even denser canopy)

This combination of criteria has proven quite effective excluding retrievals with quality issues. However, especially if the detection of senescent leaves is of interest to the user, then the LAI/Cab criteria may turn out to be problematic because in these cases the low-quality flag may not be justified. For the mixed prior extension, CRDP-2 – products contain three additional flags (bits 10, 11, and 12 listed in Table 4). Bit 12 (PRIOR_LAST_RETRIEVAL) indicates that the mixed prior approach was used and contains information from the previous retrieval. If the previous retrieval is not usable due to quality concerns, the default prior is used and bit 11 (PRIOR_UNTRUSTED) is set. If the current retrieval is invalid, the mixed prior is written to the file and bit 10 (RETR_UNSUCCESSFUL) is set. This ensures that the information from previous retrievals is retained through periods without successful retrievals. As these values are relaxed towards the default prior, they should not be seen as an actual gap-filling of the data. Especially in extreme locations (e.g. desert, rain forest), the RETR_UNSUCCESSFUL pixels should not be used or included in an analysis as they will not contain good results. Consequently, all non-parameter quantities are set to "missing" for such pixels in the intermediate files and the whole pixel will be set to missing data in the final product.

Table 4: Potential data layers in OptiSAIL output. For all quantities, the standard error and the correlation with all other main layers is given. For layers included in CRDP-2, please see the PUG (VP-CCI_D4.2_PUG).

Name	Standard/long name	Unit
Time	time (dimension)	days since 1970-01-01 00:00
Lon	Longitude (dimension)	degrees_east
lat	Latitude (dimension)	degrees_north
N_struct	PROSPECT-D leaf structure parameter	1
Cab	PROSPECT-D leaf chlorophyll a+b content	ug.cm-2
Car	PROSPECT-D leaf carotenoids content	ug.cm-2
Anth	PROSPECT-D leaf Anthocyanin content	ug.cm-2
Cbrown	PROSPECT-D leaf brown pigments content in arbitrary units	1
Cw	PROSPECT-D leaf equivalent water thickness	g.cm-2
Cm	PROSPECT-D leaf dry matter content	g.cm-2
LIDFa_II	SAIL average leaf angle (degrees) for type II	degree
LAI	SAIL Leaf Area Index	m2.m-2
hspot	SAIL hot spot parameter (av. leaf size / canopy height)	1
soilEOF1	SURF soil reflectance model parameter 1	1
soilEOF2	SURF soil reflectance model parameter 2	1
moisture	SURF relative volumetric moisture saturation of soil (theta/theta_sat)	1
snowheight	SURF snow height below canopy	m
k_vol	RossLi-reciprocal RossThick kernel parameter k_vol	1
k_geo	RossLi-reciprocal LiSparse kernel parameter k_geo	1
cloud_thk	Optical thickness from cloud contamination detection, only reporting median cloud thickness over all observations for the pixel. This was handled differently in CRDP-1.	m
*f*APAR	fraction of Absorbed Photosynthetically Active Radiation using diffuse ASTMG173	1
*f*APAR_Cab	*f*APAR absorbed by Chlorophyll-A+B	1
*f*APAR_Car	*f*APAR absorbed by Carotenoids	1
BHR_VIS	bi-hemispherical reflectance (albedo) in the visible range	1
BHR_NIR	bi-hemispherical reflectance (albedo) in the near infra-red range	1
BHR_SW	bi-hemispherical reflectance (albedo) in the shortwave range	1

DHR_VIS	directional-hemispherical reflectance (black-sky albedo), VIS, at local solar noon	1
DHR_NIR	directional-hemispherical reflectance (black-sky albedo), NIR, at local solar noon"	1
DHR_SW	directional-hemispherical reflectance (black-sky albedo), SW, at local solar noon	1
*name*_ERR	*name* standard_error	Unit of *name*
*name1_name2*_correl	*name1 name2* standard_error_correlation	1

Table 5: Quality flags as collected in "invcode" data layers in OptiSAIL output. Bits 3,7,10-31 are currently not used.

bit	value	Flag_meaning	Comment
0	1	NOT_PROCESSED	Pixel not processed (sea point or missing data)
1	2	OPTIERR_TOO_MANY_ITER	Inversion stopped at iteration limit
2	4	OPTIERR_LNSRCH	Inversion stopped for numerical reasons
4	16	XHESSERR_NOTSYM	The computed Hessian matrix is not symmetric, and uncertainties and correlations cannot be computed.
5	32	XHESSERR_INVERSION	The computed Hessian matrix cannot be inverted, and uncertainties and correlations cannot be computed.
6	64	XHESSERR_NOTPOSDEF	The computed Hessian matrix is not positive definite (e.g. if no cost function minimum was reached), and uncertainties and correlations cannot be computed.
8	256	RETR_UNTRUSTED	The retrieval is not trusted, because any of the previous bits with "ERR" in their name are raised, or the chi-square-criterion is violated.
9	512	RETR_LOW_QUALITY	The retrieval matches one or more criteria defined for low quality (see text for explanation).
10	1024	RETR_UNSUCCESSFUL	Retrieval contains previous retrieval, time-relaxed towards the standard prior, in order to bridge a missing data/or unsuccessful retrieval gap. This is no valid data for the user and is set to missing data in the final product.
11	2048	PRIOR_UNTRUSTED	Previous retrieval cannot be used for "mixed prior" approach, falling back to standard prior.
12	4096	PRIOR_LAST_RETR	Mixed-prior retrieval using previous retrieval together with standard prior

5 Selection of the input data

The optimal combination of input data is defined by analysing the retrievals for 2 years (2012 and 2019) with each different sensor availability. For each of the years, various scenarios were evaluated. Table 6 and Table 7 define the scenarios for the year 2019 and 2012 respectively.

Table 6: Scenarios to evaluate input data (2019).

No	Sensor	all	1/family	No AVHRR
1	SuomiNPP-VIIRS	X	X	X
2	NOAA20-VIIRS	X		
3	MetopA-AVHRR	X		
4	MetopC-AVHRR	X	X	
5	PROBA-V	X	X	X
6	Sentinel3-OLCI	X	X	X

MetopB-AVHRR was not considered as input data, because it shows a geolocation shift of more than 1 pixel compared to the other MetopA and C AVHRR sensors. The geolocation of these latter sensors agree well with that of Proba-V and VIIRS.

Table 7: Scenarios to evaluate input data (2012).

No	Sensor	all	No AVHRR
1	SuomiNPP-VIIRS	X	X
2	MetopA-AVHRR	X	
3	SPOT5-VGT2	X	X

Both product accuracy and processing performance are evaluated and are used to select the optimal selection of the input data. In summary and with the described settings, the 1-per-family-approach (corresponging to “all” in 2012 and similar years) appeared to give the best balance between quality and computational performace, with little or nothing to gain from the “all” scenario.

5.1 Evaluation method

5.1.1 Product quality

The quality of the different multi-sensor scenarios is assessed following the procedures described in the product validation plan [VP-CCI_D1.3_PVP_V1.1], which is compliant with the CEOS LPV recommendations (Fernandes et al., 2014). The analysis is focused on key criteria including spatial consistency, -temporal consistency, accuracy and precision of the test products. The proposed methodology relies on validation with ground-based reference (so-called direct validation) and satellite product intercomparison approaches.

The validation with ground reference is computed using three datasets:

- (DIRECT 2.1) upscaled maps (Camacho et al., 2024) following the CEOS LPV recommendations (Fernandes et al., 2014; Morisette et al., 2006) available for the year 2012 (5 sites over rice crops).
- Copernicus GBOV V2 upscaled land products, available for 2019, are also used, providing valuable multi-temporal information across 15 sites.
- AMMA sites (Redelsperger et al., 2006), where variables were derived from the acquisition and the processing of hemispherical photographs taken along 1 km linear sampling transects

The product intercomparisons are computed over the LAND VALidation (LANDVAL) network (Fuster et al., 2020; Sánchez-Zapero et al., 2023, 2020) of sites, composed of 720 sites, is used for sampling global conditions. The different multi-sensor scenarios are mainly compared with two satellite-based products for benchmarking: :

- The baseline mono-sensor CRDP-1 dataset based on SPOT/VGT (2012) and PROBA-V (2019).
- Copernicus Land Monitoring Service (CLMS) collection 1 km V2 (Verger et al., 2023). The algorithm starts from the daily SPOT/VGT or PROBA-V and instantaneous first guess of the

LAI/FAPAR variables. Then, a temporal smoothing and gap filling method is applied, using several techniques including the Savitzky-Golay filter, a climatology (Verger et al., 2013) or interpolation methods to smooth the time profile and fill the gaps.

The following criteria are analysed:

Spatial consistency: refers to the realism and repeatability of the spatial distribution of retrievals. Maps over the whole transect of different scenarios are analysed in order to check the reliability of values and to identify spatial inconsistencies for further analysis.

Temporal consistency: the realism of temporal variations is assessed over LANDVAL plus additional sites with availability of ground measurements (DIRECT 2.1, AMMA, GBOV).

Error evaluation: accuracy, precision and uncertainty (APU) of different scenarios are evaluated. Scatter-plots and validation metrics are generated for the different scenarios versus ground-based and satellite-based references for the available matchups. Additionally, the intra-annual precision (also known as smoothness, δ) (Weiss et al., 2007), which corresponds to temporal noise assumed to have no serial correlation within a season, is evaluated for the different scenarios and per biome type.

The analysis was conducted using only best quality retrievals, applying the following quality flags: RETR_UNTRUSTED (bit 8), RETR_LOW_QUALITY (bit 9), RETR_UNSUCCESSFUL (bit 10). Additionally, retrievals with p_chisquare <0.5 were filtered out.

5.1.2 Processing performance

The runtime of the processing is calculated for the tile and site processing. Statistics were derived from these per sensor combination.

5.2 Results

5.2.1 Product quality

This section presents a selection of validation results for the different scenarios.

Figure 7 illustrates the temporal dynamics of various biomes for the different scenarios for the years 2012 and 2019. A consistent seasonal behaviour, similar to that of reference products, is observed across all scenarios, with very similar values among them and most differences falling well within the uncertainty ranges.

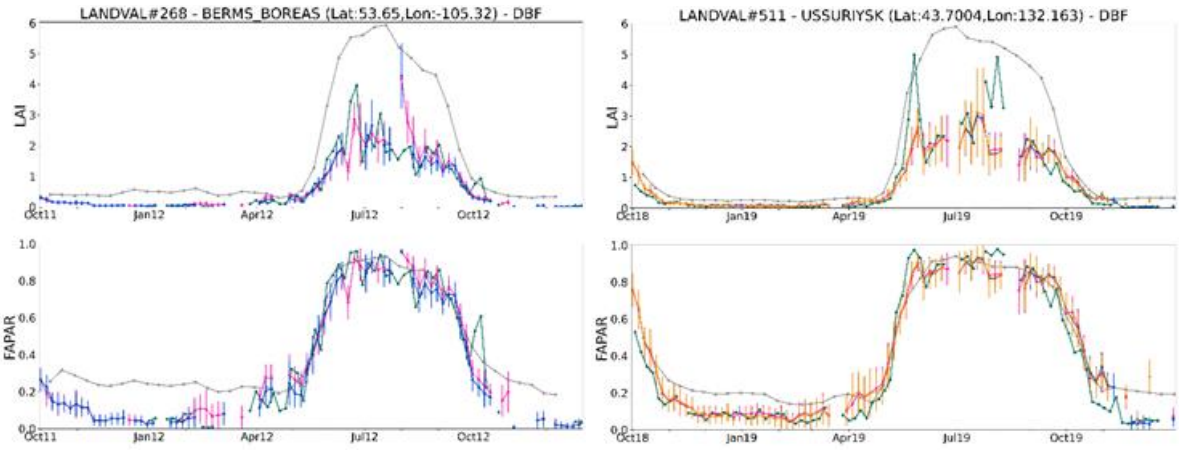

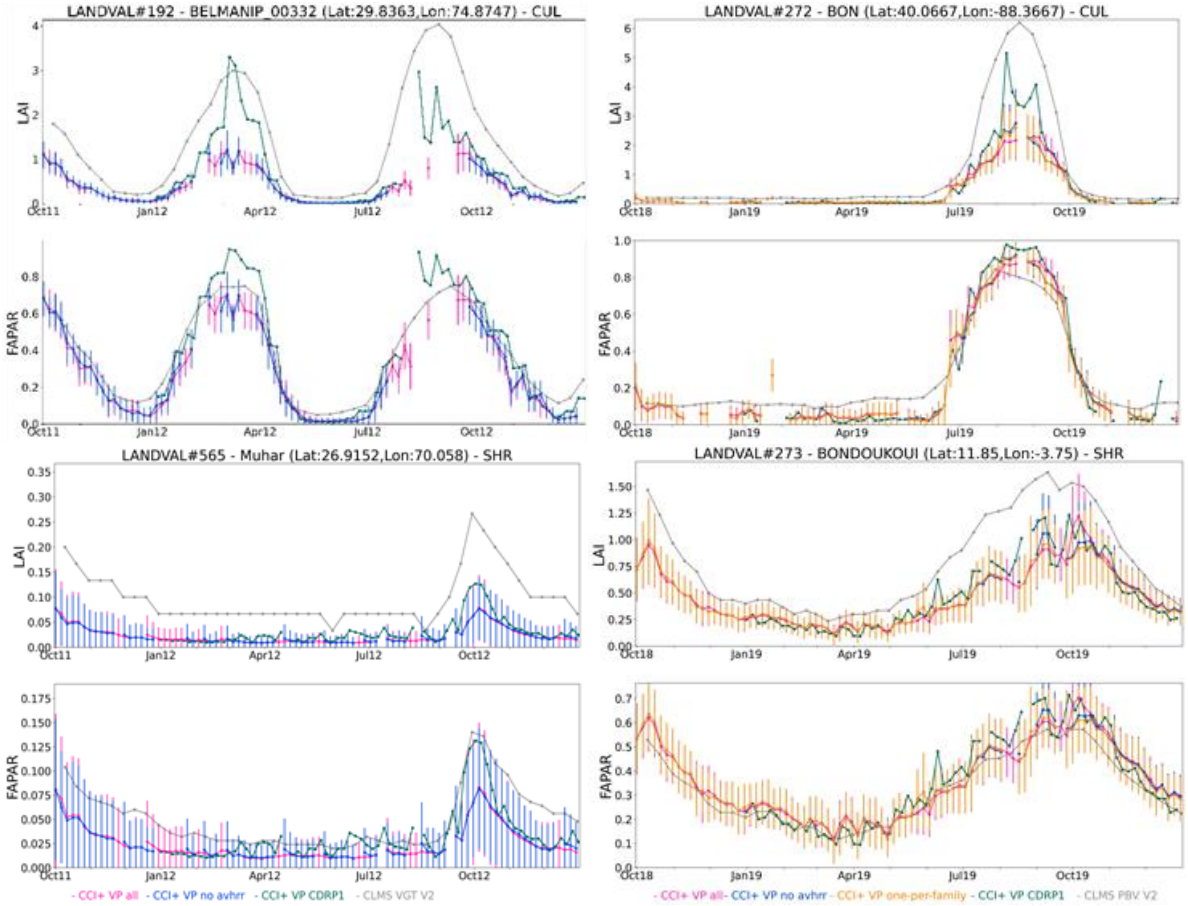

Figure 7: Temporal profiles of multi-sensor scenarios (all sensors in pink, no-AVHRR in blue, one-per-family in orange) and reference products (CDRP1 in green, CLMS V2 in grey) over selected LANDVAL Deciduous Broadleaf Forest (DBF), Cultivated (CUL) and Shrubland (SHR) sites for 2012 (left) and 2019 (right).

Figure 8 shows the median values of the intra-annual precision (smoothness, δ) for the different scenarios in 2019 over LANDVAL sites and by biome type. A significant reduction in median δ values is observed in all multi-sensor scenarios as compared to CDRP-1, particularly over forest sites. The smoothness of the multi-sensor retrievals is therefore notably better than that of the mono-sensor estimates, representing a major improvement. Conversely, there are minimal or no noticeable differences in the smoothness across scenarios, as clearly observed over LANDVAL sites. Note that the smoothness results for the 2012 scenarios yield very similar conclusions and are not shown here for the sake of brevity.

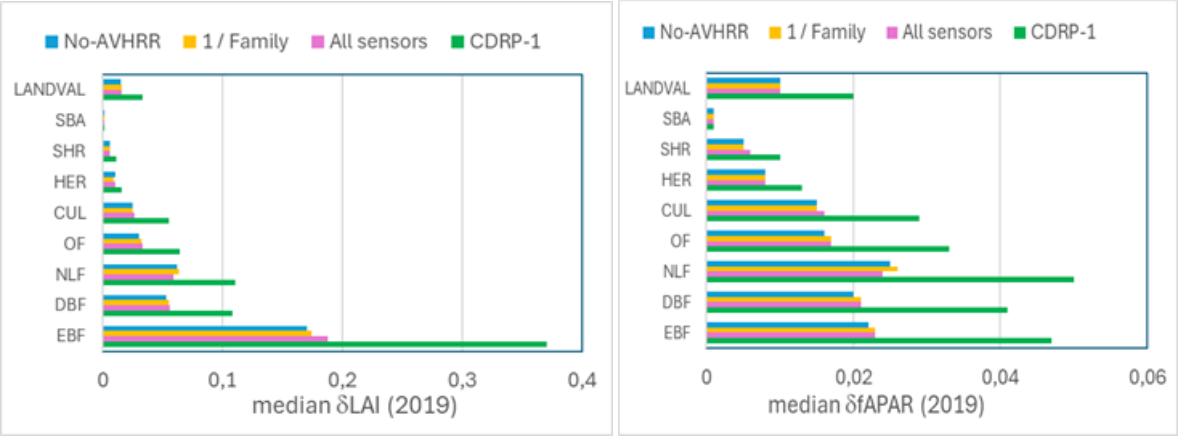

Figure 8: Smoothness (median δ values) for LAI (left side) and fAPAR (right side) for the scenarios in 2019 over LANDVAL and per biome type. The smoothness of the reference CDRP-1 data set is also included for benchmarking. SBA, SHR, HER, CUL, OF, NLF, DBF and EBF stand for Sparse and Bare Areas, Shrublands, Herbaceous, Cultivated, Other Forests, Needle-leaf Forest, Deciduous Broadleaf Forest and Evergreen Broadleaved Forest, respectively.

Figure 9 shows the scatter plot between multi-sensor LAI and fAPAR retrievals and CLMS V2 products based on SPOT/VGT for 2012. Very similar results are found for "all" and "no-AVHRR" scenarios, with almost identical validation metrics for both LAI (B=-0.79, RMSD= 1.41) and fAPAR (B=-0.04, RMSD=0.09). The larger discrepancies observed for LAI correspond to the different definitions (effective LAI versus true LAI), while good agreement is found for fAPAR, with some underestimation mainly at the highest values, where CLMS provides smoothed high values. Similar conclusions are obtained for the scenarios in 2019.

The accuracy assessment of multi-sensor scenarios with ground-based maps is shown in Figure 10. Again, very similar results are obtained regardless of the scenario (i.e., combination of sensors) considered for both LAI and fAPAR. For LAI, slightly larger correlation coefficient (R=0.87) and lower bias (B=-1.32) are obtained for the "all" sensor combination, but the difference with the other scenarios is marginal with "one-per-family" and "no-AVHRR" scenarios providing the same correlation and bias (R=0.85, B=-1.37). The large bias for LAI is again due to the different definitions between multi-sensor retrievals (effective LAI) and upscaled ground-based maps (true LAI). For fAPAR, the validation results are very good, with correlation coefficient of 0.92, very minor bias between 0.01 and 0.02 depending on the scenario, and RMSD of 0.11. There is no difference in terms of accuracy among scenarios.

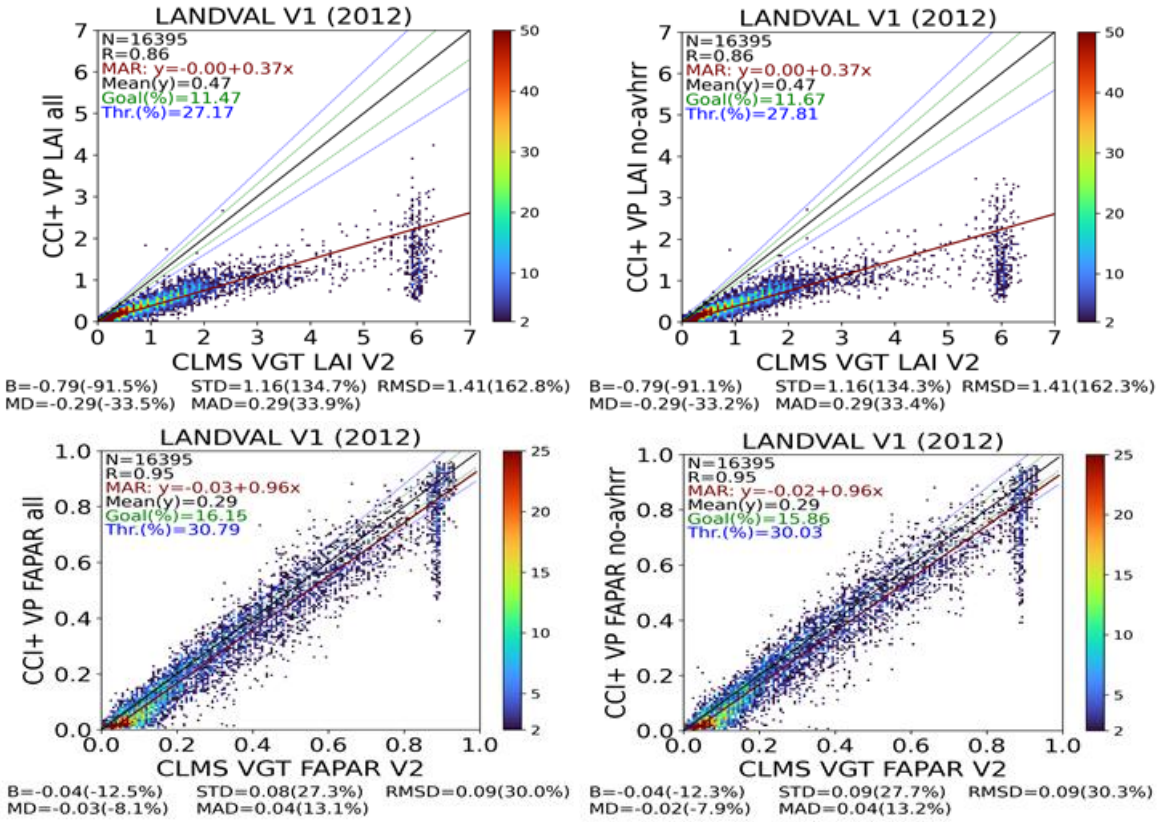

Figure 9: Scatter plots of CCI+ multi-sensor effective LAI (top) and fAPAR (bottom) against CLMS VGT V2 LAI and fAPAR products for the scenarios in 2012: All sensors (left side), No-AVHRR (right side). Computation over LANDVAL sites. Green and blue dashed lines correspond to GCOS optimal and threshold requirements on uncertainty.

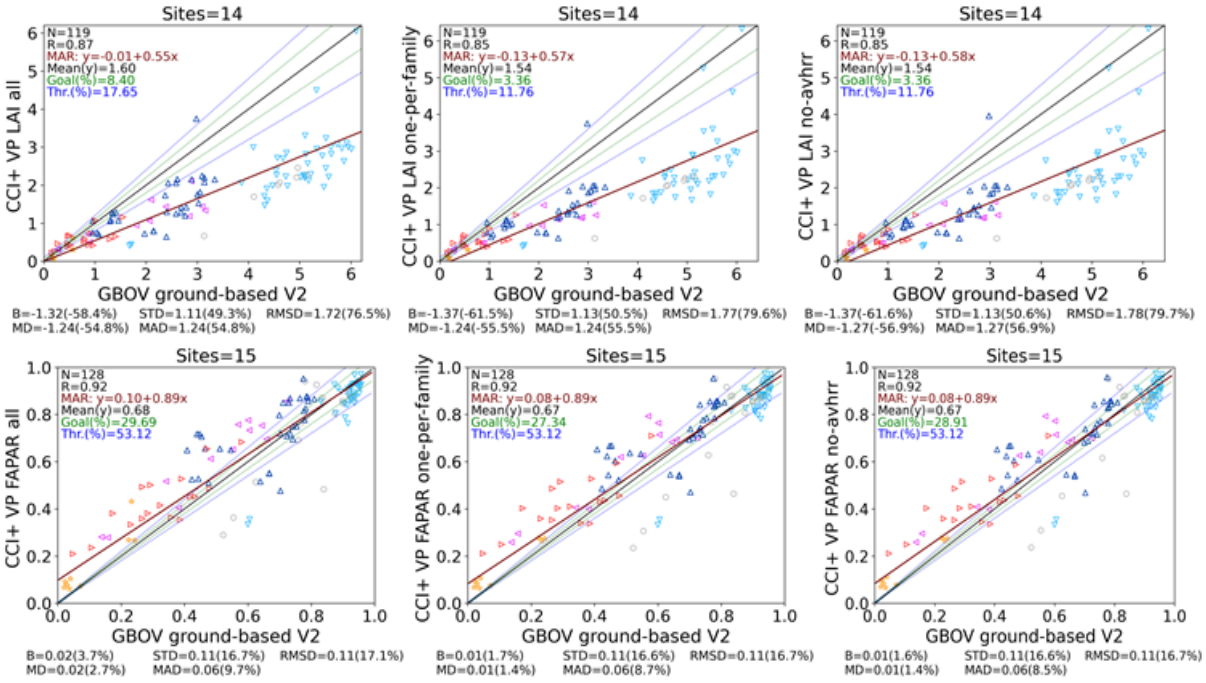

Figure 10: Scatter plots of CCI+ multi-sensor effective LAI (top) and fAPAR (bottom) versus GBOV LAI and fAPAR ground-based V2 products for the scenarios in 2019: All sensors (left), one-per-family

(middle) and no-AVHRR (right). Green and blue dashed lines correspond to GCOS optimal and threshold requirements on uncertainty.

Finally, the examination of the spatial distribution of retrievals across several tiles and periods further demonstrates that there is no apparent difference between the evaluated scenarios. An example is shown in Figure 11, where smooth transitions from low values in desertic areas in Sudan to high values in densely vegetated areas in South Sudan are observed, along with some spurious high LAI retrievals.

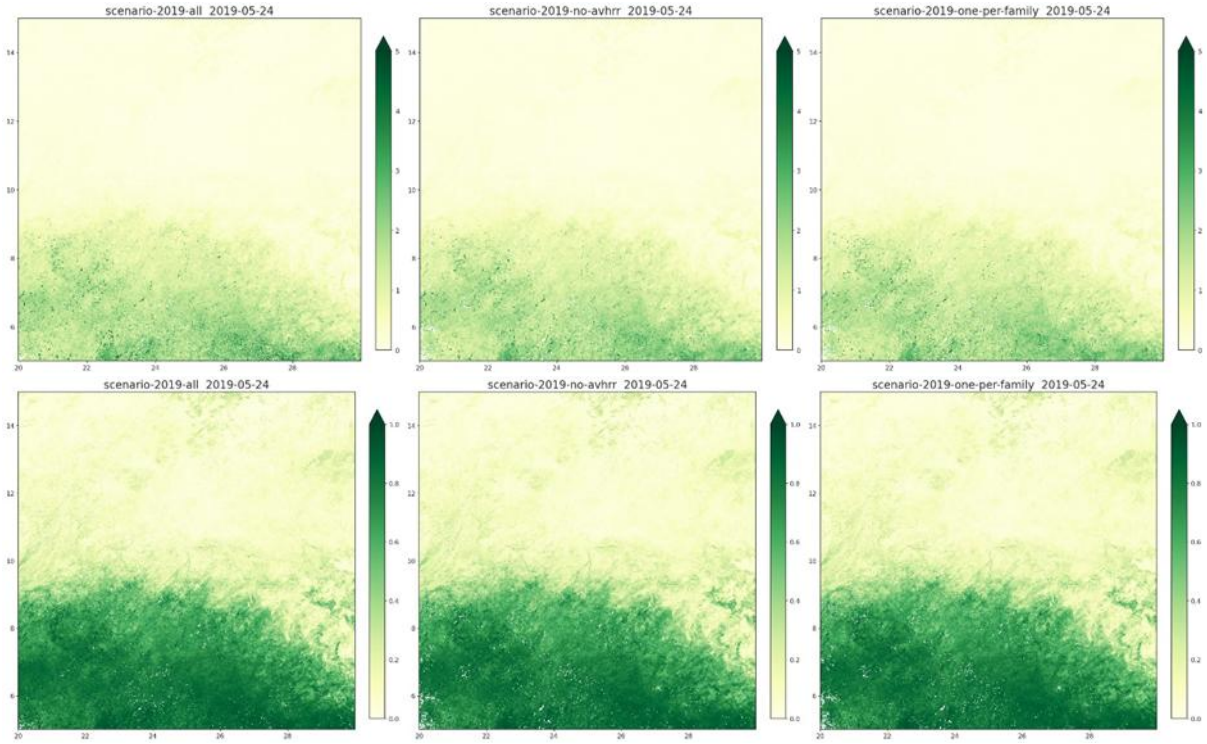

Figure 11: *Maps (tile X20Y07) of CCI+ multi-sensor LAI (top) and fAPAR (bottom) for the scenarios on 24 May 2019: All sensors (left), no-AVHRR (middle) and one-per-family (right).*

In summary, the quality of multi-sensor scenarios was tested for the 2012 and 2019 combination of sensors. In all cases, the retrievals showed good overall spatio-temporal consistency, consistent retrievals with reference satellite-based datasets, and good correlations for LAI and accurate results for fAPAR with ground-based observations. The largest improvement compared to mono-sensor retrievals has been obtained in the intra-annual precision of the products. Multi-sensor retrievals with the mixed prior approach display much better precision (smoothness) than mono-sensor retrievals, mainly over forest sites, which is the main advantage identified in this exercise (where only limited time periods of around one year were examined). On the other hand, this evaluation has shown that there are no significant differences between the different scenarios, so the evaluation of multi-sensor scenarios yields very similar results for the several input combinations, and therefore there is a little or no gain in using more sensors (“all”) rather than only a selection of them (e.g., “one-per-family”).

5.2.2 Processing performance

We assessed the processing time with the same number of executers for the different scenarios and also for the year 2000, where only VGT is available. This was done for the site and the tile processing. Table 8 summarizes the processing time for processing 1 site per scenario. Looking at the mean processing time, the processing of the year 2000 is the fastest, because only 1 sensor is available. For

the 2012 scenarios, using no AVHRR reduces the mean processing time by 2. The one per family scenario of 2019 is the fastest compared to the two other scenarios. Surprisingly, the 'no AVHRR' scenario is not faster than using all available sensors. Probably because it takes more time to find a solution for the retrieval, as also suggested by the maximum processing time. Looking at the minimum processing time, this is the same for the '1 per family' and 'no AVHRR' scenarios. As all 1243 sites can run in parallel, these statistics are also valid for processing all sites.

Table 8: Time to process 1 site per scenario

	min [hours]	max [hours]	mean [hours]	median [hours]	number of sites
scenario-2000-only-vgt	0.02	0.09	0.05	0.04	1243
scenario-2012-all	0.09	0.80	0.24	0.22	1243
scenario-2012-no-avhrr	0.04	0.46	0.12	0.10	1243
scenario-2019-all	0.16	0.71	0.35	0.34	1243
scenario-2019-no-avhrr	0.11	2.00	0.36	0.29	1243
scenario-2019-one-per-family	0.11	0.67	0.29	0.28	1243

For the current input data, there are 7 years with only VGT (scenario 2000), 6 years with the same input as used for scenarios of 2012 and 8 years for scenarios of 2019. Table 9 shows the time to process 1 site over the entire time series 2000-2020. The processing time is very similar among the different scenarios but differs in the worst-case calculations. Nevertheless, the processing time for all scenarios is feasible.

Table 9: Time to process 1 site for the full time series.

	Expected [hours]	worst case [hours]
2000-2020 all	4.59	11.11
2000-2020 no-avhrr	3.95	19.39
2000-2020 all+one-per-family	4.11	10.79

The same exercise was done for the tile-processing. Similar to Table 8, Table 10 shows the processing time to process 1 tile per scenario but leaving out the 'no AVHRR' scenario. The tile processing shows large differences in processing time between the scenarios of 2019. Using all the available sensors results in a considerable larger processing time.

Table 10: Time to process 1 tile per scenario

	min [hours]	max [hours]	mean [hours]	median [hours]	number of tiles
scenario-2012-all	4.70	10.72	8.05	8.02	23
scenario-2019-all	15.38	34.93	22.64	21.21	23
scenario-2019-one-per-family	8.57	26.15	17.02	17.18	23

Table 11 summarizes the analysis for the expected and worst-case time to process a single tile, the transect of 23 tiles or the global data (420 tiles), assuming that 15 tiles can be processed in parallel (constraint driven by the availability of processing resources and the memory consumption of the

processing chain). The processing time for the global data is a rough extrapolation, since not all tiles are equally filled with land. The results show a large impact on processing time when using all available input sensors.

Table 11: Time to process 1 tile, the transect and the global data for the full time series

	Tile		Transect		Global	
	Expected [days]	**Worst case [days]**	**Expected [days]**	**Worst case [days]**	**Expected [days]**	**Worst case [days]**
2000-2020 all	11.91	17.45	23.82	34.90	333.48	488.60
2000-2020 all+one-per-family	10.03	14.63	20.06	29.06	280.84	406.84

5.3 Conclusion

The choice was made to use the 'all + 1 per family' scenario for the processing of the output datasets as shown in Figure 12.

The analysis of the product quality did not reveal significant differences between the different scenarios. Therefore, the choice is purely based on the lower processing time for that algorithm.

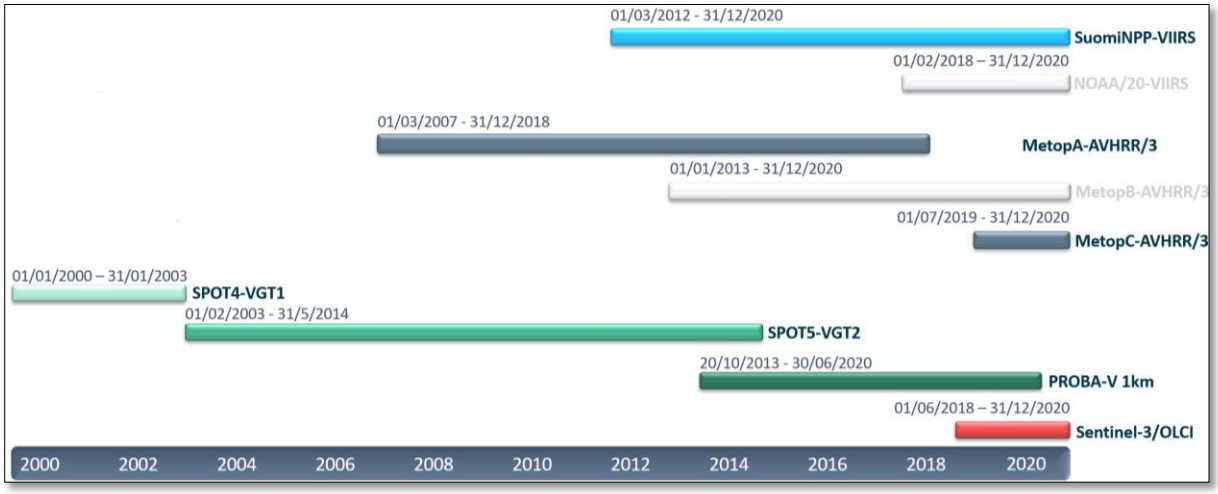

Figure 12: Selection of the input sensors for the 1 km output datasets CRDP-2 and CRDP-3. The not selected sensors are indicated in white.

6 References

Blessing, S., Giering, R., & van der Tol, C. (2024). OptiSAIL: A system for the simultaneous retrieval of soil, leaf, and canopy parameters and its application to Sentinel-3 Synergy (OLCI+SLSTR) top-of-canopy reflectances. *Science of Remote Sensing*, *10*, 100148. https://doi.org/10.1016/J.SRS.2024.100148

Camacho, F., Sánchez-Zapero, J., Fang, H., Weiss, M., Brown, L.A., 2024. CEOS LPV DIRECT V2.1: A database of upscaled LAI, FAPAR and Fcover values for satellite biophysical product validation. [Data set]. Zenodo. https://doi.org/10.5281/ZENODO.11235157

Fang, H. (2021). Canopy clumping index (CI): A review of methods, characteristics, and applications. *Agricultural and Forest Meteorology*, *303*, 108374.

Féret, J.-B., Gitelson, A. A., Noble, S. D., & Jacquemoud, S. (2017). PROSPECT-D: Towards modeling leaf optical properties through a complete lifecycle. *Remote Sensing of Environment*, *193*, 204–215. https://doi.org/10.1016/j.rse.2017.03.004

Fernandes, R., Plummer, S.E., Nightingale, J., Baret, F., Camacho, F., Fang, H., Garrigues, S., Gobron, N., Lang, M., Lacaze, R., Leblanc, S.G., Meroni, M., Martinez, B., Nilson, T., Pinty, B., Pisek, J., Sonnentag, O., Verger, A., Welles, J.M., Weiss, M., Widlowski, J.-L., Schaepman-Strub, G., Román, M.O., Nicheson, J., 2014. Global Leaf Area Index Product Validation Good Practices. Version 2.0. In G. Schaepman-Strub, M. Román, & J. Nickeson (Eds.), Best Practice for Satellite-Derived Land Product Validation (p. 76): Land Product Validation Subgroup (WGCV/CEOS), doi:10.5067/do [WWW Document]. https://doi.org/10.5067/doc/ceoswgcv/lpv/lai.002

Fuster, B., Sánchez-Zapero, J., Camacho, F., García-Santos, V., Verger, A., Lacaze, R., Weiss, M., Baret, F., Smets, B., 2020. Quality Assessment of PROBA-V LAI, fAPAR and fCOVER Collection 300 m Products of Copernicus Global Land Service. Remote Sens. 12, 1017. https://doi.org/10.3390/rs12061017

Libois, Q., Picard, G., France, J. L., Arnaud, L., Dumont, M., Carmagnola, C. M., & King, M. D. (2013). Influence of grain shape on light penetration in snow. *The Cryosphere*, *7*(6), 1803–1818.

Morisette, J.T., Baret, F., Privette, J.L., Myneni, R.B., Nickeson, J.E., Garrigues, S., Shabanov, N. V., Weiss, M., Fernandes, R.A., Leblanc, S.G., Kalacska, M., Sánchez-Azofeifa, G.A., Chubey, M., Rivard, B., Stenberg, P., Rautiainen, M., Voipio, P., Manninen, T., Pilant, A.N., Lewis, T.E., Iiames, J.S., Colombo, R., Meroni, M., Busetto, L., Cohen, W.B., Turner, D.P., Warner, E.D., Petersen, G.W., Seufert, G., Cook, R., 2006. Validation of global moderate-resolution LAI products: A framework proposed within the CEOS land product validation subgroup. IEEE Trans. Geosci. Remote Sens. 44, 1804–1814. https://doi.org/10.1109/TGRS.2006.872529

Nilson, T. (1971). A theoretical analysis of the frequency of gaps in plant stands. *Agricultural Meteorology*, *8*, 25–38.

Philpot, W. (2010). Spectral reflectance of wetted soils. *Proceedings of ASD and IEEE GRS*, *2*, 1–12.

Pinty, B., Lavergne, T., Dickinson, R. E., Widlowski, J.-L., Gobron, N., & Verstraete, M. M. (2006). Simplifying the interaction of land surfaces with radiation for relating remote sensing products to climate models. *Journal of Geophysical Research: Atmospheres*, *111*(D2).

Redelsperger, J.L., Thorncroft, C.D., Diedhiou, A., Lebel, T., Parker, D.J., Polcher, J., 2006. African Monsoon Multidisciplinary Analysis: An International Research Project and Field Campaign. Bull. Am. Meteorol. Soc. 87, 1739–1746. https://doi.org/10.1175/BAMS-87-12-1739

Sánchez-Zapero, J., Camacho, F., Martínez-Sánchez, E., Lacaze, R., Carrer, D., Pinault, F., Benhadj, I., Muñoz-Sabater, J., 2020. Quality Assessment of PROBA-V Surface Albedo V1 for the Continuity of the Copernicus Climate Change Service. Remote Sens. 2020, Vol. 12, Page 2596 12, 2596. https://doi.org/10.3390/rs12162596

Sánchez-Zapero, J., Martínez-Sánchez, E., Camacho, F., Wang, Z., Carrer, D., Schaaf, C., García-Haro, F.J., Nickeson, J., Cosh, M., 2023. Surface ALbedo VALidation (SALVAL) Platform: Towards CEOS LPV Validation Stage — Application to Three Global Albedo Climate Data Records. Remote Sens. 2023, Vol. 15, Page 1081 15, 1081. https://doi.org/10.3390/RS15041081

van der Tol, C., Vilfan, N., Dauwe, D., Cendrero-Mateo, M. P., & Yang, P. (2019). The scattering and re-absorption of red and near-infrared chlorophyll fluorescence in the models Fluspect and SCOPE. *Remote Sensing of Environment*, *232*. https://doi.org/10.1016/j.rse.2019.111292

Verger, A., Baret, F., Weiss, M., Kandasamy, S., Vermote, E., 2013. The CACAO method for smoothing, gap filling, and characterizing seasonal anomalies in satellite time series. IEEE Trans. Geosci. Remote Sens. 51, 1963–1972. https://doi.org/10.1109/TGRS.2012.2228653

Verger, A., Sánchez-Zapero, J., Weiss, M., Descals, A., Camacho, F., Lacaze, R., Baret, F., 2023. GEOV2: Improved smoothed and gap filled time series of LAI, FAPAR and FCover 1 km Copernicus Global Land products. Int. J. Appl. Earth Obs. Geoinf. 123, 103479. https://doi.org/10.1016/J.JAG.2023.103479

Weiss, M., Baret, F., Garrigues, S., Lacaze, R., 2007. LAI and fAPAR CYCLOPES global products derived from VEGETATION. Part 2: validation and comparison with MODIS collection 4 products. Remote Sens. Environ. 110, 317–331. https://doi.org/10.1016/j.rse.2007.03.001

Yang, P., Verhoef, W., Prikaziuk, E., & van der Tol, C. (2021). Improved retrieval of land surface biophysical variables from time series of Sentinel-3 OLCI TOA spectral observations by considering the temporal autocorrelation of surface and atmospheric properties. *Remote Sensing of Environment*, *256*, 112328. https://doi.org/10.1016/J.RSE.2021.112328

Zemp, M., Chao, Q., Han Dolman, A. J., Herold, M., Krug, T., Speich, S., Suda, K., Thorne, P., & Yu, W. (2022). *GCOS 2022 implementation plan*.